Coupling-induced resonance frequency shifts in coupled dielectric multi-cavity filters

Miloš A. Popović, Christina Manolatou and Michael R. Watts

Department of Electrical Engineering and Computer Science and Research Laboratory of Electronics, Massachusetts Institute of Technology, Cambridge, Massachusetts 02139
mpopovic@alum.mit.edu

Abstract: Coupling-induced resonance frequency shifts (CIFS) are theoretically described, and are found to be an important fundamental source of resonance frequency mismatch between coupled optical cavities that would be degenerate in isolation. Their deleterious effect on high-order resonant filter responses and complete correction by pre-distortion are described. Analysis of the physical effects contributing to CIFS shows that a positive index perturbation may bring about a resonance shift of either sign. Higher-order CIFS effects, the scaling of CIFS-caused impairment with finesse, FSR and index contrast, and the tolerability of frequency mismatch in telecom-grade filters are addressed. The results also suggest possible designs and applications for CIFS-free coupled-resonator systems.

©2006 Optical Society of America

OCIS Codes: (230.5750) Resonators, (130.3120) Integrated optics devices.

References and links:

1. B. E. Little, S. T. Chu, H. A. Haus, J. Foresi and J.-P. Laine, "Microring resonator channel dropping filters," J. Lightwave Technol. **15**, 998-1005 (1997).
2. S. Blair and Y. Chen, "Resonant-enhanced evanescent-wave fluorescence biosensing with cylindrical optical cavities," Appl. Opt. **40**, 570-582 (2001).
3. P. P. Absil, J. V. Hryniewicz, B. E. Little, P. S. Cho, R. A. Wilson, L. G. Joneckis and P.-T. Ho, "Wavelength conversion in GaAs microring resonators," Opt. Lett. **25**, 554-556 (2000).
4. B. Liu, A. Shakouri and J. E. Bowers, "Passive microring-resonator-coupled lasers," Appl. Phys. Lett. **79**, 3561-3563 (2001).
5. M. Lončar, T. Yoshie, Y. Qiu, P. Gogna and A. Scherer, "Low-threshold photonic crystal laser," in *Proc. SPIE* **5000**, 16-26 (2003).
6. C. K. Madsen and J. H. Zhao, *Optical filter design and analysis: a signal processing approach* (Wiley, 1999).
7. S. Fan, P. R. Villeneuve, J. D. Joannopoulos, M. J. Khan, C. Manolatou and H. A. Haus, "Theoretical analysis of channel drop tunneling processes," Phys. Rev. B **59**, 15882-15892 (1999).
8. H. A. Haus, B. E. Little, M. A. Popović, S. T. Chu, M. R. Watts and C. Manolatou, "Optical resonators and filters," in *Optical Microcavities*, K. Vahala, ed. (World Scientific, Singapore, 2004).
9. H. A. Haus, "Microwaves and Photonics," in *OSA TOPS 23 Symposium on Electro-Optics: Present and Future*, H.A. Haus, ed., (Optical Society of America, Washington, DC, 1998), pp. 2-8.
10. M. J. Khan, C. Manolatou, S. Fan, P. R. Villeneuve, H. A. Haus and J. D. Joannopoulos, "Mode-coupling analysis of multipole symmetric resonant add/drop filters," IEEE J. Quantum Electron. **35**, 1451-1460 (1999).
11. A. Melloni and M. Martinelli, "Synthesis of direct-coupled-resonators bandpass filters for WDM systems," J. Lightwave Technol. **20**, 296-303 (2002).
12. R. Orta, P. Savi, R. Tascone, and D. Trinchero, "Synthesis of multiple-ring-resonator filters for optical systems," IEEE Photonics Technol. Lett. **7**, 1447-1449 (1995).
13. C. Manolatou, M. A. Popović, P. T. Rakich, T. Barwicz, H. A. Haus and E. P. Ippen, "Spectral anomalies due to coupling-induced frequency shifts in dielectric coupled-resonator filters," in *Proceedings of Optical Fiber Communication Conference on CD-ROM* (Los Angeles, CA, February 2004), TuD5.
14. T. Barwicz, M. A. Popović, P. T. Rakich, M. R. Watts, H. A. Haus, E. P. Ippen and H. I. Smith, "Microring-resonator-based add-drop filters in SiN: fabrication and analysis," Opt. Express **12**, 1437-1442 (2004), http://www.opticsexpress.org/abstract.cfm?URI=OPEX-12-7-1437.
15. M. A. Popović, M. R. Watts, T. Barwicz, P. T. Rakich, L. Socci, E. P. Ippen, F. X. Kärtner and H. I. Smith, "High-index-contrast, wide-FSR microring-resonator filter design and realization with frequency-shift compensation," in *Proc. Optical Fiber Comm. Conf.* (Optical Society of America, Washington, DC, 2005).

16. H. A. Haus, *Waves and fields in optoelectronics* (Prentice-Hall, Englewood Cliffs, NJ, 1984).
17. H. A. Haus and W.-P. Huang, "Coupled-mode theory," in *Proc. IEEE* **79**, 1505-1518 (1991).
18. T. Barwicz, M. A. Popović, M. R. Watts, P. T. Rakich, E. P. Ippen and H. I. Smith, "Fabrication of add-drop filters based on frequency-matched microring resonators," submitted to J. Lightwave Technol.
19. M. Popović, "Complex-frequency leaky mode computations using PML boundary layers for dielectric resonant structures," in *Proceedings of Integrated Photonics Research* (Washington, DC, June 17, 2003).
20. A. D. Berk, "Variational principles for electromagnetic resonators and waveguides," IRE Trans. Antennas Propag., April 1956, pp. 104-111.
21. H. A. Haus, W. P. Huang and A. W. Snyder, "Coupled-mode formulations," Opt. Lett. **14**, 1222-1224 (1989).
22. C. Manolatou, M. J. Khan, S. Fan, P. R. Villeneuve, H. A. Haus and J. D. Joannopoulos, "Coupling of modes analysis of resonant channel add-drop filters," IEEE J. Quantum Electron. **35**, 1322-1331 (1999).
23. M. J. Khan, M. Lim, C. Joyner, T. Murphy, H. A. Haus and H. I. Smith, "Integrated Bragg grating structures," in *Digest of the LEOS Summer Topical Meeting on WDM Components* (Copper Mountain, CO, 2001).
24. J. Scheuer and A. Yariv, "Two-dimensional optical ring resonators based on radial Bragg resonance," Opt. Lett. **28**, 1528-1530 (2003).
25. A. Yariv, "Universal relations for coupling of optical power between microresonators and dielectric waveguides," Electron. Lett. **36**, 321-322 (2000).
26. S. V. Boriskina, T. M. Benson, P. Sewell and A. I. Nosich, "Effect of a layered environment on the complex natural frequencies of 2D WGM dielectric-ring resonators," J. Lightwave Technol. **20**, 1563-1572 (2002).
27. B. E. Little, J.-P. Laine and S. T. Chu, "Surface-roughness-induced contradirectional coupling in ring and disk resonators," Opt. Lett. **22**, 4-6 (1997).
28. M. M. Lee and M. C. Wu, "MEMS-actuated microdisk resonators with variable power coupling ratios," IEEE Photon. Technol. Lett. **17**, 1034-1036 (2005).

1. Introduction

High-Q dielectric resonators, like microrings and photonic crystal micro-cavities, are enabling the use of microphotonic circuits for filtering, sensing, nonlinear interaction and lasers [1-5]. Complex, high-order resonant structures, of importance for bandpass channel add-drop filters, dispersion elements or slow-wave structures [1, 6-12], are formed by coupling multiple optical cavities. The spectral response is engineered by the choice of resonance frequencies of, and coupling strengths between, the constituent cavities. Therefore, command of the resonance frequencies in design is important. For example, in series-coupled-cavity filters [1, 10-12], flat-top bandpass responses call for identical uncoupled cavity resonances, where the choice of coupling strengths (set by appropriate coupling gaps) determines the particular response shape. Such examples suggest a geometry employing physically identical resonators, or in Vernier schemes, different-sized cavities with coincident uncoupled resonances.

In this paper, we show that coupling of cavities introduces self-coupling perturbations that give rise to new *effective uncoupled resonance frequencies*, leading to severe response impairments that must be corrected in design. In Ref. [13], we reported initial findings on coupling-induced resonance frequency shifts (CIFS). Here, we give the first more complete treatment and discussion. We first demonstrate the effect of CIFS on filter response by rigorous numerical eigenmode and finite-difference time-domain (FDTD) simulations. The simulations show that accounting for CIFS is necessary and sufficient for simplified transfer-matrix and coupled-mode models, supplemented by numerically computed coefficients, to accurately match full FDTD simulation results for a third-order microring-resonator filter. Next, we call upon coupled-mode theory to qualitatively explain the effect, and discuss the physical basis and rigorous evaluation of CIFS in traveling-wave and general resonators. Counter to what may be expected for positive-index perturbations, we show that CIFS can be of negative or positive sign. By compensating for the predicted shift, we verify that the ideal filter response may be recovered. We then analyze the scaling of the effect with index contrast, inter-cavity cross-coupling strength, bandwidth and free spectral range (FSR). Finally, we discuss CIFS-free coupled resonator designs and comment on generic methods of compensation for CIFS.

Resonant frequency mismatch is particularly deleterious to in-band extinction in the through port of high-order add-drop filters [14, 15]. The results show that it must be
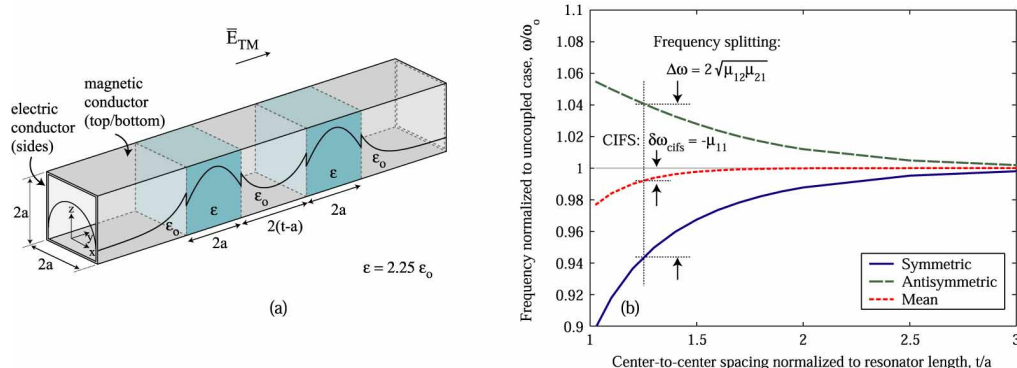
Fig. 1. (a) Coupled-dielectric-resonator system in infinite perfect-conductor waveguide, with analytic mode solutions [17]; (b) TM$_{10}$ supermode frequency splitting and CIFS vs. resonator spacing.

accounted for in the filter design in order to achieve the desired symmetric high-extinction responses that will enable the use of resonator-based filters in channel add-drop applications.

For the sake of clarity, we reiterate that CIFS is a coupling effect in linear systems and refers to a perturbation of the resonance property of the electromagnetic cavity and *not* to a shift in frequency of an input signal.

2. CIFS and its effect in multipole resonators

Before demonstrating its deleterious effect on a multipole resonator, we define CIFS through a simple example. An idealized two-cavity system in Fig. 1(a), of identical dielectric blocks in an infinite conducting waveguide, has an analytic TM$_{10}$-mode solution (cf. [17]). Coupling results in a frequency splitting $\Delta\omega$ [Fig. 1(b)] of the supermodes [16, 17]. It also causes a shift $\delta\omega$ in the mean supermode frequency. The latter may be interpreted as a coupling-induced shift in *effective* uncoupled resonance frequencies, that we refer to as CIFS.

In higher-order resonators based on multiple cavities, engineering supermode poles directly is difficult. A more tractable design framework is based on individual cavity modes and uncoupled cavity resonance frequencies, with separate coupling and CIFS terms to describe the coupled configuration. Thus, the individual cavity design and the coupling design are made, to a large extent, independent.

The dynamics of the system are described by coupling of modes in time (CMT) [16, 17],

$$\frac{d}{dt}\vec{a} = j\overline{\overline{\boldsymbol{\omega}}} \cdot \vec{a} - j\overline{\overline{\boldsymbol{\mu}}} \cdot \vec{a} \qquad (1)$$

where the amplitudes $\vec{a}$ are associated with the resonant modes and normalized such that $|a_n|^2$ is the energy of mode n; $\overline{\overline{\boldsymbol{\omega}}}$ is a diagonal matrix of uncoupled resonance frequencies, and matrix $\overline{\overline{\boldsymbol{\mu}}}$ represents mode coupling. Off-diagonal elements $\mu_{i,j}$ represent cavity-to-cavity coupling employed in engineering the supermodes. Diagonal elements $\mu_{i,i}$ represent CIFS and modify $\overline{\overline{\boldsymbol{\omega}}}$ into effective cavity resonance frequencies. Solving (1) yields frequency splitting,

$$\omega_{s,a} = \frac{\omega_1 - \mu_{11} + \omega_2 - \mu_{22}}{2} \mp \sqrt{\left(\frac{(\omega_1 - \mu_{11}) - (\omega_2 - \mu_{22})}{2}\right)^2 + \mu_{12}\mu_{21}} \;. \qquad (2)$$

CIFS ($\mu_{i,i}$) is a second-order, self-coupling effect, as compared to the direct coupling $\mu_{i,j}$ that is first-order, leads to frequency splitting [Fig. 1(b)] and sets the bandwidth. On the other hand, in *spectral response* models, CIFS is contained linearly, as a modification of resonance frequency, while cross-coupling is squared [1]. In net result, the two effects are comparable.
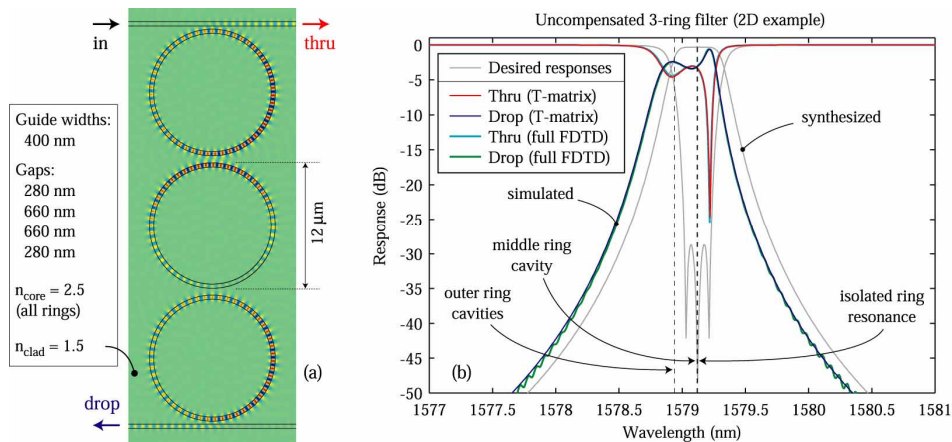
Fig. 2. CIFS impairment of 3-cavity microring filter: (a) simulated structure using identical rings (dimensions shown); (b) ideal (synthesized) and simulated (complete-structure FDTD and model) frequency response showing apparent cavity mismatch due to CIFS.

A two-dimensional (2D) simulation demonstrates that CIFS can seriously impair a filter design. A channel add-drop filter, based on a series-coupled 3-ring resonator, was synthesized to have a 50GHz 3dB passband and 30dB in-band extinction in the through port [1, 11]. The microring resonators are identical and hence degenerate in the absence of coupling, with 3200 GHz FSR near 1580nm. The required power coupling coefficients are {0.0825, 0.00155, 0.00155, 0.0825}, corresponding to coupling gaps of {280, 660, 660, 280} nm. FDTD simulation of the complete filter was carried out to find the drop and through port spectral responses. For completeness, details of the simulations are given in Appendix A. A snapshot of the field in the simulated structure is shown in Fig. 2(a), and the desired (synthesized) and obtained (simulated) filter responses are shown in Fig. 2(b). The ideal synthesized response is obtained by a transfer-matrix-method computation [6, 12] assuming matched resonators. The asymmetric simulated response is a telltale sign of resonance frequency mismatch due to CIFS [13]. To account for the observed response shape in theory, a mismatch of ~22GHz (on the order of the filter bandwidth) must be supposed. The response is so severely distorted that, mid-band, the signal is split evenly between the drop and through ports rather than being dropped. As shown below, this distortion is the net effect only of varying CIFS contributions in the three cavities caused by their coupling configurations. Experimentally determining CIFS is complicated by additional fabrication-related resonance frequency offsets between cavities that can be comparable to the CIFS, and add to the response distortion [18].

CIFS distortion and compensation is illustrated in Fig. 3, starting with an isolated resonant cavity, here a microring resonator [Fig. 3(a)]. Placing a cavity near a waveguide or near a second resonant cavity, results in coupling through the perturbation of the evanescent fields that extend outside the dielectric core region. In addition to the coupling, the changed proximate environment that perturbs the evanescent field of a cavity causes a CIFS. For an arbitrary filter coupling coefficient distribution, the perturbation seen by the mode of each resonator will, in general, be different in accordance with the arrangement of perturbing nearby structures "seen" by its evanescent field [Fig. 3(b)]. When assembled in a higher-order filter, the effective resonance frequency of each cavity is shifted from its value in isolation [Fig. 3(c)]. Since the shifts are in general not identical, the system response is not only shifted in frequency, but also distorted. To recover the desired response, the cavities may be pre-distorted in design so that in the complete filter, the *effective uncoupled resonance frequencies* are again degenerate [Fig. 3(d)].
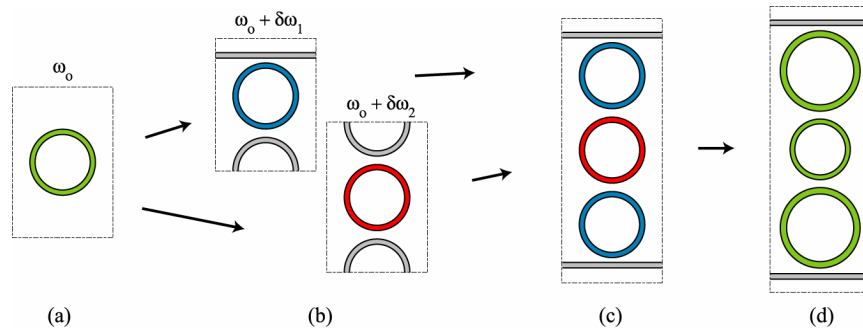
Fig. 3. Diagram of CIFS resonance mismatch and its correction: isolated resonator (a) attains CIFS when part of a coupled structure (b); the combination of nominally degenerate resonators in a coupled-cavity filter (c) results in effectively mismatched resonators and a distorted response (Fig. 2), which can be corrected by pre-distorting the resonators by the expected CIFS

3. Physical sources and the sign of CIFS in general resonators

We next consider the rigorous evaluation and the physical origin of contributions to CIFS leading to shifts of either sign. Then, we demonstrate CIFS in traveling and standing-wave resonators and note characteristic field patterns associated with positive and negative shifts.

Resonant modes of an isolated dielectric electromagnetic cavity [Fig. 3(a)], or those of the compound resonator [Figs. 3(c) and 3(d)], may be computed numerically using a complex-frequency mode solver [19]. Since the supermode pole distribution of a compound resonator is the result of two effects – frequency splitting and (pair-wise) mean frequency shifting (CIFS) – it is more desirable to set up the computation problem so as to separate these two effects. We partition the complete multi-cavity filter geometry into sub-structures [Fig. 3(b)], each selecting one resonance in the spectrum of interest associated with a cavity mode. This approach enables a series of numerical mode simulations to yield isolated CIFS and coupling parameters for each cavity.

A complex-frequency eigenmode solution [19] provides the resonance frequencies and corresponding quality factors, Q's, of the simulated (sub)structure's resonant modes. In each partitioned sub-structure, supermode splitting due to buildup of energy in a second resonance is eliminated, since only one resonance in the frequency range of interest is present. In this way the effect of CIFS on each cavity may be evaluated. One may further separate CIFS contributions due to each of the interacting objects by individual simulations. Each perturbation is small and physically isolated so the total shift is, to a good approximation, the sum of the individual isolated contributions. The Q's, on the other hand, encompass not only radiation and absorption losses, but also power coupled out of the resonator via waveguides. By properly taking guided-mode overlap integrals at access waveguide ports with the complex resonant-mode field, the total Q may be decomposed into an external coupling Q and a loss Q.

In Fig. 4, the CIFS due to adjacent bus waveguides is evaluated by eigenmode computation for a ring resonator identical to those in Fig. 2. Two symmetrically coupled bus waveguides are more efficiently simulated by exploiting the horizontal and vertical axis symmetry. Each waveguide contributes half of the total CIFS, found as the difference between the computed resonant frequency of the coupled, and that of the uncoupled resonator. The CIFS is plotted (in free-space wavelength units) against ring-waveguide gap spacing, and for two bus waveguide widths and polarizations for a resonance nearest 1580nm. As expected, the magnitude of the frequency shift decreases for increasing gap width with an exponential envelope, due to the exponential tails of the interacting evanescent fields.

The sign of the frequency shift requires more attention. A small positive refractive index perturbation is typically expected to cause a negative frequency shift. The three simulated cases in Fig. 4 were chosen, however, to point out that the CIFS may be negative or positive, depending on geometry (here the bus waveguide width) and even on the polarization. The CIFS sign depends on contributions from effects beyond first-order index perturbation,

including non-orthogonal cross-energy between the resonant mode and confined modes in nearby structures, and resonant-mode shape modification by the adjacent structures. We now enter a brief discussion of these points.

The framework of coupling of modes in time (CMT), introduced phenomenologically in Eq. (1), is instructive for obtaining insight into the physical contributions to the net CIFS of a cavity mode in the coupled configuration. CMT can provide a rigorous treatment [17] of the interaction of a collection of modes in a coupled dielectric resonator structure of arbitrary geometry. Evolution of the mode amplitudes $\vec{a}(t)$, in a suitably formulated CMT (Appendix B), may be described by a variation of the coupled-mode equations of the form of eqn. (1):

$$\frac{d}{dt}\vec{a} = j\overline{\overline{\omega}}\cdot\vec{a} - j\overline{\overline{W}}^{-1}\cdot\overline{\overline{M}}\cdot\vec{a} = j\overline{\overline{\omega}}\cdot\vec{a} - j\overline{\overline{\mu}}\cdot\vec{a} \qquad (3)$$

In addition to the uncoupled resonant-frequency diagonal matrix $\overline{\overline{\omega}}$, $\overline{\overline{W}}$ is the energy non-orthogonality (basis mode overlap) matrix, and $\overline{\overline{M}}$ is a customary coupling overlap matrix that describes the interaction. Matrices $\overline{\overline{W}}$ and $\overline{\overline{M}}$ depend on the particular formulation of CMT as reduced from Maxwell's equations (c.f. [17]; another is described in Appendix B). Regardless of the particular formulation of the CMT, the matrix $\overline{\overline{\mu}}$ represents a total effective coupling matrix with respect to mode amplitudes taking energy non-orthogonality into account. For example, in the case of two coupled resonators as in Fig. 1, the CIFS for the resonator associated with amplitude a_1 of two total modes is, according to Eq. (3) (Fig. 3):

$$\delta\omega_1 = -\mu_{11} = -\frac{M_{11} - \frac{W_{12}}{W_{22}}M_{21}}{W_{11} - \frac{W_{12}}{W_{22}}W_{21}}. \qquad (4)$$

In the absence of coupling, such as when the resonators are spaced sufficiently far apart, $\delta\omega_1 = 0$ and the resonators oscillate at their uncoupled natural frequencies in $\overline{\overline{\omega}}$. With coupling present, the CIFS is generally non-zero. We briefly consider the physical
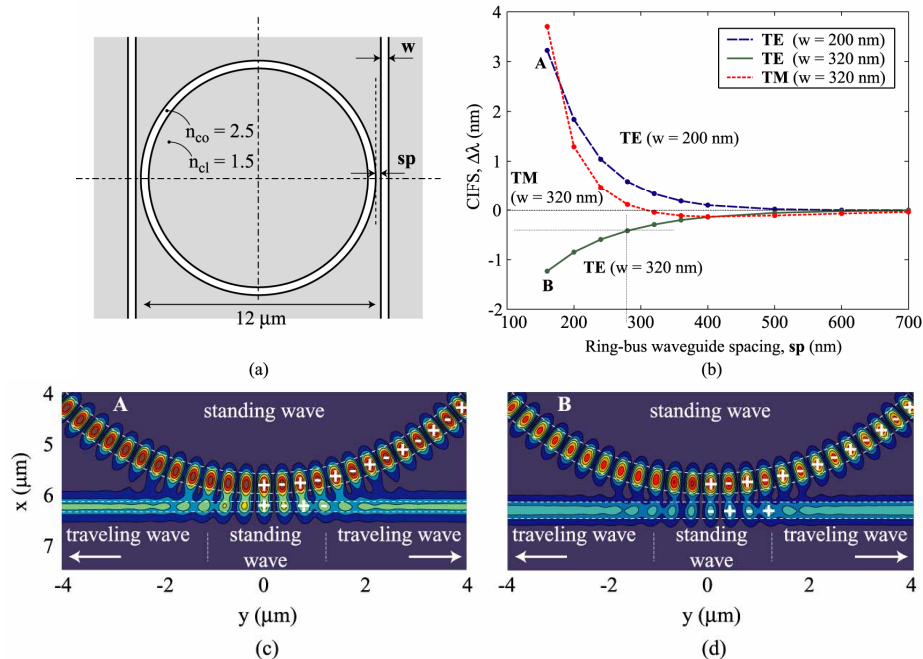

Fig. 4. CIFS in a single-ring cavity due to side-coupled bus waveguides: (a) mode-solver-simulated structure; (b) CIFS for TE, TM resonances and for two bus widths, vs. gap spacing. Phasor-amplitude plots (c), (d) of the standing-wave-mode resonant field show a partial standing wave in the coupling region and, respectively, a symmetric-like and antisymmetric-like supermode formed with the waveguide continuum corresponding to negative- and positive-frequency CIFS.
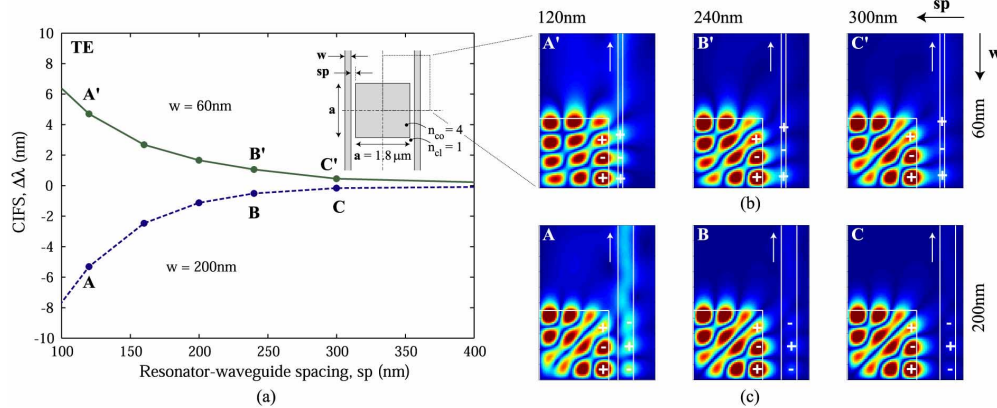
Fig. 5. CIFS due to coupled bus waveguides in a square standing-wave cavity: (a) CIFS vs. gap spacing and waveguide width, and mode-solver simulated structure. Mode phasor magnitude plots show (b) symmetric and (c) anti-symmetric coupling, respectively, with a partial standing wave established in the waveguide, for negative- and positive-frequency CIFS. Case (b) shows significant mode shape modification caused by coupling.

interpretation of (4). For a basis of orthogonal modes (e.g. a lone resonator perturbed by a nearby dielectric object with no relevant modes of its own) $W_{12} = W_{21} = 0$, and from (4) the frequency shift is negative since M_{ii}/W_{ii} is positive definite in the lossless case. This is an intuitive result if one considers the wave equation or its stationary integral for frequency (lossless case) [20]:

$$\omega^2 = \frac{\int_V \vec{E}^\dagger \cdot \nabla \times \overline{\overline{\boldsymbol{\mu}}}^{-1} \cdot \nabla \times \vec{E} \ dv}{\int_V \vec{E}^\dagger \cdot \overline{\overline{\boldsymbol{\epsilon}}} \cdot \vec{E} \ dv}. \tag{5}$$

If a positive refractive index perturbation is introduced to the isolated cavity configuration in (5), the frequency must decrease. In the case of adjacent evanescently-coupled resonators, the basis of uncoupled modes that are subjected to coupling is normally not orthogonal. A second, positive CIFS contribution then arises due to the cross-energy of the modes. Since cross-coupling M_{21} (source of power exchange) is a large term relative to self-coupling M_{11}, the net CIFS could be found positive. This initially unintuitive result is more easily understood in the spatial-propagation picture in Sec. 4, specific to traveling-wave resonators.

One final comment with respect to the CMT treatment is in order. In a rigorously derived CMT, meaningful estimates of the first-order coupling (supermode splitting) can be obtained from overlap integrals, with the error converging to zero with weaker coupling as expected. However, the diagonal elements representing CIFS are second-order coupling effects, and are not accurately predicted by CMT formulations, including [17, 21]. An error in the uncoupled field basis representation of the supermode field solution also translates to a second-order contribution to the CIFS, similar to the analogue in the spatial picture of directional couplers [21]. Such an error will always be present in practice, when a finite basis of modes is selected. Therefore, the relative error in the CIFS estimate by CMT does not converge to zero with weaker coupling and can in general be $\mathcal{O}(1)$. This is the case because CMT is fundamentally a first-order theory. So, while valuable physical insight may be gained, CMT does not generally provide an accurate estimate of the CIFS. For design purposes, an accurate determination is obtained by using a resonator mode solver (Fig. 2) or the FDTD method.

The general resonance treatment in time (by CMT or exact frequency eigenmode methods) is useful because it applies to all types of resonators, including standing wave resonators such as dielectric box-type resonators [22] and side-coupled, quarter-wave shifted waveguide grating resonators [23], photonic crystal cavities [5, 7], annular Bragg resonators [24], etc. For example, CIFS vs. gap width for a square resonator is shown in Fig. 5(a), computed by the

frequency mode solver. A 2D model structure with 4:1 index contrast and 1.8μm edge dimension supports a high-Q mode with diagonal field nulls [22] at 1559.6nm, with a radiation Q of 203,000. Choices of bus waveguide width produce a positive or negative CIFS.

Finally, an interesting observation may be made with respect to the symmetry of characteristic field patterns for resonator interaction with the bus waveguide. It is generally appreciated that coupling of two degenerate resonators splits modes such that the symmetric supermode is of lower resonant frequency and the anti-symmetric is higher. In the case of resonator-waveguide coupling only one resonant mode is present, but it may be observed that the symmetry of the interaction of the resonator mode with a partial standing wave established over a portion of the waveguide still determines the character of the resonance frequency modification and thus the sign of the CIFS. In Figs. 5(b) and 5(c) the field phasor amplitude is plotted over a quarter of the simulated structure for two different waveguide widths. A traveling-wave (uniform-intensity) pattern is seen in the waveguide away from the interaction region, signifying leaking power associated with Q-broadening, but a more standing-wave-like pattern is seen in the immediate coupling region. In Fig. 5(b), the anti-symmetric standing wave pattern in the coupling region corresponds to a positive-frequency (negative-wavelength) CIFS, while in Fig. 5(c) the symmetric interaction pattern corresponds to a negative-frequency CIFS. This behavior is present also in the ring resonator [Figs. 4(c) and 4(d)].

4. Coupling-induced frequency shifts in traveling-wave-resonator structures

We next treat CIFS in traveling-wave resonators, such as microring resonators; relate the frequency shift to phase perturbations in couplers; investigate a coupler model and the constraints imposed by power conservation; and take a coupling-of-modes in space look at CIFS.

Traveling-wave resonators are particularly useful because they support high Q's and permit unidirectional coupling to waveguide modes. They couple to access waveguides or other resonators via directional coupler regions. The coupling may be evaluated by considering each coupling region as a multi-port within particular reference planes [1-4 in Fig. 6(a)]. Reflection in these interaction regions can be neglected, so that the responses of filters using ring resonators can be obtained by a transfer matrix analysis considering only unidirectional forward wave scattering [6, 12].

CIFS may be attributed to a phase shift in propagation [from port 4 to port 3 in Fig. 6(a)] due to interaction in the directional coupler regions. A round-trip net phase shift of 2π (a full wavelength) would shift the resonance by one full FSR, so the CIFS is related to the phase as,

$$\frac{\Delta f_{CIFS}}{\Delta f_{FSR}} \approx \frac{\Delta f_{CIFS} n_g L}{c} \approx -\frac{\Delta \phi}{2\pi}. \tag{6}$$

where L is the round-trip cavity length and n_g is the group index of the traveling-wave mode. The phase perturbation $\Delta \phi$ is explicitly manifest in the scattering or S-matrix, $\overline{\overline{U}}$, of a lumped, point-interaction description of the coupler in Fig. 6(a) (note that in fact $\overline{\overline{U}}$ is an off-diagonal 2×2 submatrix of the total 4-port scattering matrix, since reflection and backward transmission are neglected). In general, the interaction is distributed over an extended length of propagation where the fields in the traveling wave cavity and nearby coupled structure are "within reach" of each other's evanescent tails. The net effect on relevant modes may be evaluated with respect to reference planes [1-4 in Fig. 6(a)] that sufficiently enclose the interaction region. However, it is instructive to lump the distributed interaction into a point interaction with respect to a single reference plane, represented by a point S-matrix, $\overline{\overline{U}}$. Then, propagation along the remainder of the structure in the interaction region is treated as that in the uncoupled structures. This partitioning, without loss of generality, simplifies analysis to that of isolated resonators, plus lumped point interactions. The lumped interaction matrix displays only the frequency dependence of the coupling interaction itself (and not of the propagation/dynamical phase), as seen in Fig. 6(b). In addition, loss due to propagation (e.g. in bent waveguides constituting the rings) and any excess loss caused by the interaction are
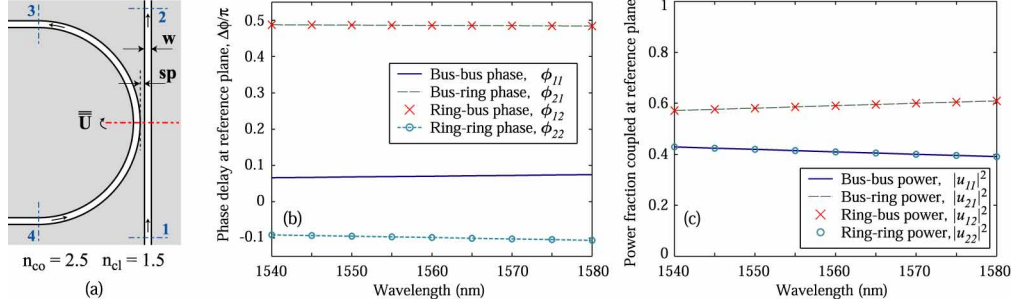
Fig. 6. (a) Lumped point-interaction model of coupling of traveling-wave resonator and access waveguide. FDTD simulation of the coupled structure with respect to ports 1-4, and of the two waveguides individually, leads to lumped point-interaction matrix **U**, describing the effect of the coupling on port-to-port scattering matrix element (b) phase, and (c) power coupling.

separated. In our simulations, we obtain the point S-matrix $\overline{\overline{U}}$ by evaluating the S-matrix with respect to reference planes 1-4 of the coupled structure in Fig. 6(a), as well as that of the uncoupled ring and bus waveguides. The latter permit normalizing the uncoupled propagation phase and loss out of the former to obtain a point scattering S-matrix $\overline{\overline{U}}$ [referenced to the red plane in Fig. 6(a)] which represents the perturbation due to interaction.

Power conservation constraints on the point S-matrix of a lossless directional coupler permit sufficient latitude in degrees of freedom to support two independent coupling-induced phase offsets that correspond to the CIFS. A lossless coupler with two inputs, two outputs and no reflection to input ports may be represented by an arbitrary unitary 2×2 transfer matrix $\overline{\overline{U}}$ with four degrees of freedom – a power coupling ratio κ, and three phases θ_o, θ_1, θ_2:

$$\overline{\overline{U}} \equiv \begin{vmatrix} u_{11}e^{i\phi_{11}} & u_{12}e^{i\phi_{12}} \\ u_{21}e^{i\phi_{21}} & u_{22}e^{i\phi_{22}} \end{vmatrix} = e^{i\theta_o} \begin{vmatrix} \sqrt{1-\kappa}e^{i\theta_1} & i\sqrt{\kappa}e^{i\theta_2} \\ i\sqrt{\kappa}e^{-i\theta_2} & \sqrt{1-\kappa}e^{-i\theta_1} \end{vmatrix} \tag{7}$$

where $\vec{b} = \overline{\overline{U}} \cdot \vec{a}$, $\vec{b} \equiv [b_2, b_3]^T$, $\vec{a} \equiv [a_1, a_4]^T$ [Fig. 6(a)] and $\overline{\overline{U}}$ is referenced to a single input-output reference plane. The unitary condition, $\overline{\overline{U}}^{\dagger}\overline{\overline{U}} = \overline{\overline{I}}$, alone requires that the phases obey

$$\phi_{11} + \phi_{22} = \phi_{21} + \phi_{12} \pm \pi \tag{8}$$

which is explicitly satisfied by the second form in (7). In the absence of coupling, $\kappa \to 0$ and phases $\theta_{0,1,2} \to 0$, such that $\overline{\overline{U}} \to \overline{\overline{I}}$ (identity matrix) and uncoupled behavior is recovered. In the presence of coupling, κ represents power coupling and $\theta_0 \pm \theta_1$ are two independent coupling-induced phase shifts on either side due to interaction, which translate to frequency shifts in resonant elements. For a coupler that is symmetric about a (horizontal) axis separating the input and output ports [Fig. 6(a)], reciprocity combined with the geometric symmetry requires equal off-diagonal elements, i.e. $\theta_2 \to 0$, reducing the number of free parameters to three. But, the two diagonal coupling-induced phase shifts remain independently determined, permitting two different CIFS values for resonators on each side of the coupler.

Figures 6(b) and 6(c) show the FDTD computation of the elements of matrix $\overline{\overline{U}}$ for the ring and bus waveguide structures used in the filter example of Fig. 2. A narrower coupling gap of 100nm is used in order to amplify and make clearly visible the phase shifts due to interaction. Figure 6(c) shows power coupling (cross state ~60%) and its wavelength dependence due to change in mode confinement. The total output power sums to >99.9% for even smaller coupling gaps and supports this discussion using the unitary matrix model. Figure 2(b) shows the phase shifts, which by inspection can be seen to, and were verified to, obey condition (8). The cross-state phase shifts are equal and near 90º as expected. However, it is interesting to note that the bar-state phase shifts on the bus and ring sides are large and of

opposite sign ("anomalous" and normal, respectively). This is a manifestation of the multiple contributions to the CIFS, discussed in the temporal resonance picture previously and briefly further discussed below. It implies that, for example, when coupling two resonators of different radii such as in a Vernier scheme (c.f. [1]), it is possible for the two to experience CIFS of opposite signs.

For the filter example of Fig. 2, using computed phase shifts for the appropriate coupling gaps, Eq. (6) and the cavity FSR, a CIFS of +21.75 GHz results due to each bus waveguide and a CIFS of +0.26 GHz due to each adjacent ring (note, CIFS here has the "anomalous" sign). A net mismatch results of +21.49 GHz in outer rings relative to the middle ring. These CIFS values were used in the filter model plotted in Fig. 2, and give a response that matches exactly the FDTD-simulated response of the complete filter, also plotted and overlapping. The "wiggles" in the wings of the FDTD-simulated drop spectrum below -30dB are due to a slightly premature termination of the simulation. A step-function turn-off of the field leaving the drop-port while some energy remains in the computational domain causes small oscillations in the shown spectrum obtained by discrete Fourier transform (DFT) of the output field. Rigorous accounting for CIFS is thus necessary and sufficient to explain the anomalous spectrum obtained in Fig. 2.

Transfer-matrix-type analyses of lossless ring-resonator filter couplers (c.f. [12, 6, 25]) have generally employed the unitary scattering matrix of a two-port mirror (c.f. [16]), which is consistent also with first-order coupling-of-modes in space analysis of a directional coupler ([16], p.220). These have one less degree of freedom than the model in Eq. (7) because the reference planes for input (incident) and output (reflected) waves of each port are generally coincident, unlike the 4-port reflectionless couplers considered here, where the planes may be arbitrarily chosen. Secondly, while the S-matrix phase variables may be removed by a particular choice of reference planes, in general such choices hold at a single frequency only [16], and do not provide the intuitive physical picture of the interaction obtained by collocating all four reference planes. By placing the interaction at a point and treating the remainder of the propagation as that in an uncoupled resonator, the perturbative nature of the interaction on the resonator is explicitly manifest in the forward scattering matrix $\overline{\overline{U}}$ of the directional coupler, including CIFS. This is a practical approach for resonant filter design.

4.1. Coupling of modes in space picture

In view of the opposite sign of coupling-induced phase shifts on the ring and bus side of the coupler in Fig. 6, we briefly revisit the physical sources of CIFS in a spatial picture. For traveling wave resonators, the CIFS may be simply understood by using a coupling of modes in space [16,17] approach to consider the self-phase-shift accumulated in directional couplers. First, the propagation constant β_i of waveguide i is modified to $\overline{\beta_i} = \beta_i + \delta\beta_i$ by the diagonal term $\delta\beta_i$ of a coupling matrix analogous to $\overline{\overline{\mu}}$ in the temporal system of Eqs. (1) or (3), e.g.:

$$\delta\beta_1 = \frac{K_{11} - \frac{P_{12}}{P_{22}} K_{21}}{P_{11} - \frac{P_{12}}{P_{22}} P_{21}} \tag{9}$$

where $\delta\beta_1$ is given for mode 1 of two modes and may in general vary in value along the propagation direction, $\overline{\overline{K}}$ is the coupling overlap matrix and $\overline{\overline{P}}$ is the non-orthogonality matrix as in [17]. For perfectly synchronous couplers, this is the only coupling-induced phase contribution and the accumulated phase is the integral of $\delta\beta_i(z)$ along the propagation direction over the interaction region, with CIFS given by (6). In general, at least parts of a coupling region may be non-synchronous, and then additional phase is accumulated in each waveguide due to beating in the mismatched coupler. The total accumulated phase is obtained by considering the phase of the total integrated CMT solution [16] for bar-state propagation through a coupler. For a uniform coupler along the propagation direction, the total phase is
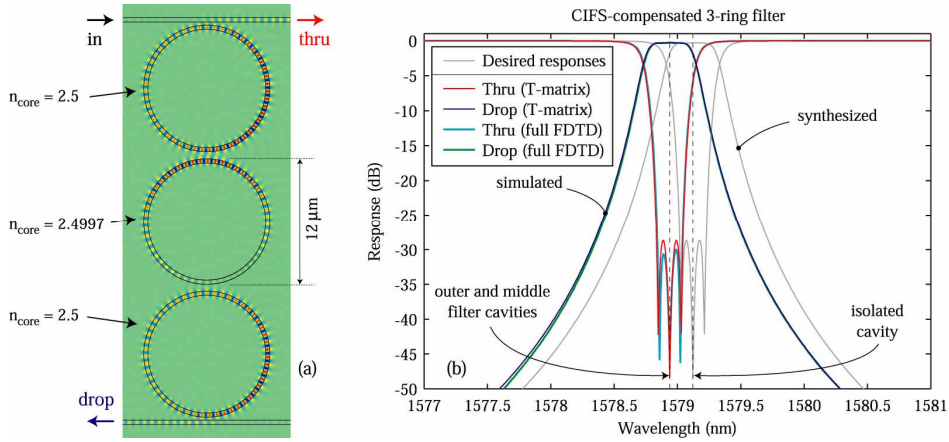
Fig. 7. FDTD simulation of 3-cavity microring filter, with cavity resonance frequencies pre-compensated by design for CIFS: (a) simulated structure with lower-core-index middle ring; (b) FDTD simulation and model of the filter showing recovered ideal frequency responses.

$$\Delta\theta_1 = \beta_1 z + \delta\beta_1 z + \left[\delta z - \arg\{\cos(\beta_o z) + j\frac{\delta}{\beta_o}\sin(\beta_o z)\}\right] \qquad (10)$$

where $\delta \equiv (\bar{\beta}_2 - \bar{\beta}_1)/2$, $\beta_o \equiv \sqrt{\delta^2 + \bar{\kappa}^2}$ and $\bar{\kappa}^2 \equiv \bar{\kappa}_{21}\bar{\kappa}_{12}$. Non-orthogonal couplings $\bar{\kappa}_{21}, \bar{\kappa}_{12}$ are off-diagonal elements of $\bar{\bar{P}}^{-1} \cdot \bar{\bar{K}}$. In gradual couplers where synchronism, propagation constant and coupling vary with length along the propagation direction, the terms in (10) contain integrals with respect to distance. The three phase terms on the right-hand side of (10) are due to the uncoupled β, the coupling-induced β shift, and the non-synchronous slip phase. The latter two terms result from coupling and contribute a CIFS according to (6). The third term may be significant when asynchronous (asymmetric or bent) and interferometric couplers are employed. For synchronous ($\delta = 0$), strongly asynchronous ($|\delta| \gg |\bar{\kappa}|$), or optically short ($|\bar{\kappa}|z \ll 1$) couplers, no significant amount of power is coupled over and back with phase slip, and the second term in (10) is the dominant contribution.

Even without phase slip due to asynchronous coupling, this picture confirms that the CIFS can be of either sign. K_{11} is the usual positive effective index (negative CIFS) contribution due to the presence of the high index adjacent bus waveguide or resonator. The second term in (9) that gives a positive CIFS contribution can be understood by considering two weakly guided TE coupled slabs of half the width necessary to cut off the second guided mode. At zero wall-to-wall spacing (strong coupling regime), the two guides merge and the antisymmetric mode becomes cut off, while the symmetric mode morphs into the fundamental guided mode. In approaching this situation, clearly the antisymmetric mode's effective index drops much faster than that of the symmetric mode rises. This example clarifies the negative contribution to the average effective index of the two supermodes, seen in Fig. 4 and Fig. 6, which for synchronous coupled waveguides corresponds to a $\delta\beta < 0$ in (9), or a CIFS > 0.

5. Compensation of CIFS in design

The frequency mismatch due to CIFS, observed in the filter in Fig. 2, can be compensated by pre-distorting the resonance frequencies of the isolated cavities in design, in anticipation of CIFS shifts. This may constitute slight cavity geometry or index modifications. In general, the pre-distorted cavity design will, in the coupled configuration, have a slightly different CIFS than the original, so that iteration would be needed to arrive at a self-consistent design. In practice, a single step is adequate. The cavity resonance frequency is sufficiently sensitive to dimensional or index changes that a small modification can produce a resonance shift equal

to the CIFS without substantially affecting the mode shape, and thus the coupling and CIFS. In addition, the cavity may be modified only away from the interaction region.

Figure 7 shows the simulation of a compensated filter. Recalling the example of Fig. 2, the outside rings had a CIFS of +21.75 GHz, and the middle ring +0.26 GHz. For the compensated filter, the core index of the middle ring was changed by -0.0003 to compensate for the net CIFS of -21.49 GHz in the middle ring by causing a frequency shift equal in magnitude, and opposite in sign (resonance shifts -7.11 GHz/0.0001 core index change). Index, rather than dimensional, perturbation is used on account of the coarse discretization, but the results can be trusted as explained in Appendix A. The simulated filter responses show the flat-top Chebyshev passband that was desired, with 30dB in-band extinction (slight asymmetry shows ~0.2GHz residual mismatch). A transfer-matrix-method model, incorporating the individually modeled couplers and no net CIFS is overlaid confirming agreement. Coupler computations using FDTD and the modesolver (external Q) yield virtually identical results. The simulation confirms that CIFS was the only unaccounted impairment in the example filter of Fig. 2, and that its proper compensation enables the realization of the ideal filter response. In this example, only the net CIFS was compensated by modifying the middle ring, so the compensated filter center frequency remains slightly blue-shifted [Fig. 7(b)]. This is sufficient because filters are generally desired to be tunable as a unit. Furthermore, in practice the center frequency is sensitive to variations and difficult to control. But in general, we may compensate all resonators to rigorously recover the exact desired response. Fabrication techniques allowing compensation of frequency shifts by pre-distortion are addressed in Ref. [18].

6. Higher-order CIFS effects

A second, higher-order CIFS-related effect in traveling-wave resonators deserves mention and may, at least in principle, impact performance. Traveling-wave resonators operate on the principle of two frequency-degenerate standing-wave resonances that are excited 90⁰ out of phase to give unidirectional propagation. It has been shown that, based on this interpretation, traveling-wave-cavity-like filters can be mimicked by properly engineered pairs of standing-wave cavities [7, 10]. However, when a traveling-wave cavity is placed near a bus waveguide or a second cavity, the symmetry is broken and the two standing wave modes of the ring resonator may no longer be degenerate [19, 26]. CIFS for the even and odd standing-wave mode with respect to the coupling symmetry axis, are in general different and will cause the splitting. A simple picture is given by the CMT-in-time treatment: the index perturbation of a bus waveguide has large overlap with the single field lump of the even mode, but smaller overlap with the odd mode which has a field null at the point of closest proximity of the coupled structures. Because the standing-wave modes are non-degenerate, the traveling-waves are no longer resonant eigenmodes of the system. From the traveling wave viewpoint, the directional coupler is a periodically phase-matched scatterer into the backward propagation direction, thus building up the reverse resonance and splitting the supermodes. In practice, this splitting is small as it is a difference of CIFS for the two similar standing-wave modes. However, sidewall-roughness-induced contra-directional coupling has been predicted to lead to deleterious resonance splitting [27]. CIFS splitting due to couplers is much smaller than the CIFS itself and the filter bandwidth, but it may impact one's ability to reach high extinction levels in higher-order filters. CIFS splitting will be greatest in high-index-contrast cavities with tight bend radii (e.g. in silicon waveguides), where the difference of overlap integrals can be more pronounced. A solution here is to make a longer, weaker directional coupler that covers several propagation wavelengths of the ring mode, thus making the overlaps more similar and the difference smaller; or, to distort the resonator shape, e.g. a ring into a slightly ellipse-shaped resonator, to compensate for the splitting of the standing-wave modes.

7. CIFS scaling laws and CIFS-free resonator configurations

Detuning of a cavity resonance impairs the response of a multi-cavity filter if the detuning is of the order of the filter bandwidth. Thus, a CIFS-to-bandwidth ratio (CBR) best expresses

scaling of the CIFS impairment with bandwidth and FSR, coupling geometry, index contrast, filter order. Through-port notch responses are particularly sensitive to variations [Fig. 2(b)], because they rely on precise suppression of the poles by zeros over the stopband. Using simple filter models [1], we find that a CBR must be well under 1/10 to avoid impairing high-extinction through-ports, independent of filter order $N > 1$.

For a fixed coupling geometry (gaps adjustable to vary bandwidth, but cavity/waveguide shapes fixed within coupling region), the CBR due to cavity-bus coupling is *independent* of bandwidth and FSR (globally scaled for all cavities). For cavity-cavity coupling it scales as

$$CBR_{cavity-cavity} \sim \left. \frac{BW}{FSR} \right|_{\text{fixed coupling geometry}} = \frac{1}{finesse} \tag{11}$$

We infer this using overlap integrals (14),(15) (or *E*-field overlaps in [17]) and the CMT model (3), and assuming evanescently coupled generic cavities. We retain only the basic index perturbation term M_{11}/W_{11} in μ_{11} [Eq. (4)], disregarding the other terms as they are of same order. These contributions may cancel to make μ_{11} smaller or zero in magnitude [Fig. 4(b)], but the first term gives a reasonable scaling for extremal values.

To relate the coupling coefficients to bandwidth scaling, we note that the bandwidth of a high-order filter is determined by resonance splitting $\sim \mu_{i,j}$ [Eq. (2)], and by line broadening $\mu_i^2 = \omega_o/Q_i$. Both are of the order of the bandwidth, so in flat-top bandpass filters the desired cavity-cavity coupling is second-order in cavity-bus coupling, $\mu_{i,j} \sim \mu_i^2$. For traveling-wave cavities, the FSRs are related as $\mu_i^2 = \kappa_i^2 FSR_i$, $\mu_{i,j}^2 = \kappa_{i,j}^2 FSR_i FSR_j$ for cavity-bus and cavity-cavity couplings [1].

Referring to an example cavity pair in Fig. 1, the self-coupling overlap integral that determines CIFS, M_{11}, depends on the overlap of the evanescent tail of cavity 1 field squared over the second cavity's core. Cavity-cavity coupling M_{21}, on the other hand, is first-order in the evanescent tail of the first cavity. Thus $M_{11} \sim M_{21}^2$ as gap is varied. This leads to the dependence (11). A similar consideration, and the different scaling of bandwidth with μ_i leads to the different conclusion for cavity-bus coupling. More generally, the CIFS for a cavity scales inversely with the FSR of adjacent cavities, but does not scale with FSR changes of the cavity itself (for constant bandwidth and coupling geometry).

The coupling geometry may also be varied for a fixed bandwidth and FSR. We assume synchronous couplers. For a fixed total coupling, the CIFS (and CBR) for a cavity scales as $1/L_{eff}$, the effective coupling length to either a cavity or bus waveguide,

$$CBR \sim \frac{\phi_{11}}{\kappa} = \frac{1}{L_{eff}} \sim \left. \sqrt{\frac{\alpha}{R_{eff}}} \right|_{\text{fixed BW,FSR}} \tag{12}$$

This also results from (15), where $M_{11} \sim M_{21}^2$ as gap is varied, while both M_{11}, M_{21} are linear in interaction length (area). For straight parallel directional couplers, L_{eff} is the length. For curved couplers (such as ring-bus waveguide couplers), the diverging coupler's curvature may be represented as a single effective radius $1/R_{eff} = 1/R_1 + 1/R_2$ [1]. Then, the effective length goes as $\sqrt{R_{eff}/\alpha}$, where α is the evanescent decay rate. Hence, a short, strong coupling region gives a larger CIFS than a long, weak one providing the same coupling. This compares a ring and a racetrack resonator. Curved coupling regions will generally be nonsynchronous, so a more accurate comparison requires consideration of non-synchronous phase slip in Eq. (10).

Higher index contrast cavity designs generally employ shorter, stronger couplers. Thus, CIFS will generally be larger in HIC designs of an equivalent bandwidth and FSR. For example, a higher group index n_g in HIC means that a smaller microring radius is required for a given FSR ($FSR = c/2\pi R n_g$), leading to a shorter stronger coupler, and greater CBR.

In some filters, including series-coupled resonators, not all cavities may need to be compensated. From the coupling coefficient relationship $\mu_{i,j} \sim \mu_i^2$ for flat-top filters, we may conclude that the cavities that are coupled to access waveguides contribute a greater CIFS

than "interior" cavities coupled only to other adjacent cavities. From (11), this will be particularly true in high-finesse filters. To first order, compensating only the outermost rings may thus be sufficient. In our example (Fig. 7), only the central ring was compensated instead.

Simple cavity design pre-distortion may not be sufficient in device designs where the resonant frequencies must remain unchanged over a range of dynamically variable coupling gap configurations, such as with MEMS-actuated switching of ring filters [28]. In these cases, a CIFS-free resonator design is desirable. Observing Fig. 4(b) or Fig. 5(a), it is evident that there exists a bus waveguide width where the CIFS is flattened to first order to near zero for all coupling gaps. Such designs may be of value where the cavity is not tunable.

8. Conclusions

Coupling-induced resonance frequency shifts were shown to arise in dielectric cavities, and to lead to severe impairment of multi-cavity filter responses in the absence of proper compensation in design. While series-coupled microring filters were used as an example, CIFS is present in other cavity types and multipole-filter geometries. CIFS is second order in coupling as gap spacing is varied, and is greater in short, strong coupling regions. The CIFS-to-bandwidth ratio is independent of bandwidth and FSR due to cavity-bus waveguide coupling, and scales as *1/finesse* due to cavity-cavity coupling. Theory and rigorous simulations show that CIFS can be positive or negative depending on the dominant of a number of contributing factors including index perturbation, mode non-orthogonality and mode field distortion. Standing- and traveling-wave pictures of the CIFS were considered. A perturbative lossless directional coupler model contains all necessary, and just enough, degrees of freedom to describe CIFS in traveling-wave cavities. A typical microring-resonator filter without CIFS compensation had a severely distorted simulated response. With CIFS compensation, the ideal synthesized response was recovered and verified by simulation. Therefore, CIFS must be rigorously taken into account in filter design, in cases where the resonator frequencies cannot be individually tuned post-fabrication. CIFS-free resonators may be engineered to enable applications such as MEMS-actuated coupling strength control via gap change, without shifting the resonance.

Appendix A. Simulation methods and case study details

Details of the simulated examples are given here to enable one to reproduce the results, and to justify the prediction of small frequency shifts by coarsely-discretized simulations.

The ring resonator was designed to have a high-Q TE resonance in the C-band with an odd round-trip number of wavelengths. The former was desired to unambiguously ensure that any spectral distortion in all examples is due to CIFS only, because far-field interference due to radiation loss may also cause a skew in the response spectrum. The latter is important because the ring is not perfectly circular in the discretized computational domain. An odd resonance still has degenerate standing wave modes, thus supporting traveling wave operation as in an ideal ring; while an even resonance has slightly split standing-wave modes so that the grid discretization causes some backward wave coupling. The circular ring resonator has a 6 μm outer radius, and a waveguide width of 400 nm with a core index of 2.5 and a cladding index of 1.5. The simple indices were chosen to permit the 2D model to approximately correspond to typical radii and FSRs (3.2 THz) seen in high-index-contrast SiN or Si filters [1, 14, 15].

Ring resonant modes and Q's, relevant to the discretized computational domain, were computed by a complex-frequency mode solver [19], solving the scalar wave equation (in the case of TE modes) on the 2D domain. Perfectly-matched-layer (PML) boundary conditions were used in the form of complex coordinate stretching, to absorb outgoing radiation and

permit the computation of leaky (finite Q) resonances. The Q is ~260k in the discretized domain (due to "grid roughness"), while the ideal ring structure has Q ~10^9.

The directional coupler interaction regions (Fig. 6), and the complete filters (Figs. 2,7) were simulated by 2D resonant mode solver and FDTD. Bus waveguides were also 400nm wide, and the ring-bus and ring-ring coupling gaps were 280nm and 660nm, respectively.

The FDTD simulation of directional couplers involved three simulations: a simulation of the coupler, a simulation of the ring section alone, and a simulation of the bus section alone. The lumped point-coupler scattering parameters referenced to the single (red) reference plane are obtained from the scattering parameters referenced to planes on the walls of a box, of the three simulations above. Couplers were virtually lossless for all gaps, including contact.

All simulations used discretization of $\Delta x = \Delta y = 20$ nm. The FDTD timestep was shorter than the CFL stability timestep by 1.1. The filter simulation was run for 1.5M timesteps for Fig. 2 (3M timesteps for Fig. 7). Wiggles in the response below -30dB in Fig. 2 are due to premature termination in time of the simulation. Such large discretization cannot determine the absolute resonance frequencies with an error smaller than the CIFS. However, the relative frequencies, such as shifts caused by coupling (relevant to CIFS), are accurately defined. The resonators in the example of Fig. 2 and Fig. 7 are made identical to remove discretization effects.

Appendix B. Vector-field coupled mode theory in time derivation

A number of derivations of the coupled-mode theory in time are possible, starting from Maxwell's equations, depending on the starting equation and choice of uncoupled basis modes. The approach in Ref. [17] gives the form (3) for degenerate cavities. In the general case, it does not explicitly show the perturbation and has a slightly more complicated form than Eqs. (3) and (4). While the details are beyond the scope of this paper, we outline briefly one general-case vector-field formulation consistent with (3) and (4) for completeness. At the same time, we choose a basis of H-fields of the uncoupled resonator modes. The E-fields may be derived from the curl equation of the total system. A choice of H-field basis set then ensures that Gauss' law is preserved in the supermode trial fields of the coupled configuration. Starting from the vector-wave equation for the total H field,

$$\nabla \times \overline{\overline{\varepsilon}}^{-1} \cdot \nabla \times \vec{H} = \omega^2 \overline{\overline{\mu}} \cdot \vec{H} \tag{13}$$

the orthogonality condition is found from the adjoint operator. We write the total dielectric distribution for each basis function n as the distribution $\overline{\overline{\varepsilon}}_n^{-1}$ for which it is an eigenmode plus a perturbation: $\overline{\overline{\varepsilon}}^{-1} \equiv \overline{\overline{\varepsilon}}_n^{-1} + \overline{\overline{\Delta\varepsilon}}_n^{-1}$ in (13). We project out the coupling matrix subsequently by applying the orthogonality condition on the equation. To make the matrices consistent with (3), we pre- and post- multiply the orthogonality matrix by a diagonal frequency matrix:

$$W_{mn} \equiv \frac{\omega_n}{\omega_m} \iiint_{\tilde{V}} \vec{H}_m^T \cdot \overline{\overline{\mu}} \cdot \vec{H}_n \; d\tilde{v} \tag{14}$$

where both fields are unconjugated to allow for leaky modes. Accordingly the tilde indicates an integration domain extending into the complex plane. The coupling matrix is similarly,

$$M_{mn} \equiv \frac{\omega_n}{2} \iiint_{\tilde{V}} \vec{D}_m^T \cdot \overline{\overline{\Delta\varepsilon}}_n^{-1} \cdot \vec{D}_n \; d\tilde{v} \, . \tag{15}$$

We have shown this formulation to give results for ring-to-ring resonator coupling that are consistent with FDTD simulations [8].